AGU PUBLICATIONS

JGR

Journal of Geophysical Research: Oceans

RESEARCH ARTICLE

10.1002/2015JC011157

Modulation of sea surface temperature warming in the Bay of Biscay by Loire and Gironde Rivers

X. Costoya[1], D. Fernández-Nóvoa[1], M. deCastro[1], F. Santos[1,2], P. Lazure[3], and M. Gómez-Gesteira[1]

[1]EPHYSLAB, Environmental PHYsics LABoratory, Facultad de Ciencias, Universidad de Vigo, Ourense, Spain, [2]CESAM, Departamento de Física, Universidade de Aveiro, Aveiro, Portugal, [3]IFREMER, Physed-DYNECO, Laboratory Physique HYdrodynamique et SEDimentaire, Centre de Bretagne, Plouzané, France

Key Points:
- The oceanic area of the Bay warms while the coastal area suffers a cooling
- The mere presence of a freshwater layer is able to modulate the warming
- Cooling is reinforced during periods with higher river discharge and SW winds

Correspondence to:
X. Costoya,
xurxocostoya@uvigo.es

Citation:
Costoya, X., D. Fernández-Nóvoa, M. deCastro, F. Santos, P. Lazure, and M. Gómez-Gesteira (2016), Modulation of sea surface temperature warming in the Bay of Biscay by Loire and Gironde Rivers, *J. Geophys. Res. Oceans*, *120*, doi:10.1002/2015JC011157.

Received 21 JUL 2015
Accepted 24 DEC 2015
Accepted article online 30 DEC 2015

Abstract The influence of Loire and Gironde River discharges over the sea surface temperature (SST) in the eastern Bay of Biscay (0.6°–36.6°W, 44.2°–47.8°W) was analyzed by means of two complementary databases (MODIS and $OISST_{1/4}$). The area influenced by river plume showed a different SST when compared with the adjacent oceanic area for the months when the plume attains its highest extension (December, January, and February). Ocean was observed to warm at a rate of approximately 0.3°C dec^{-1} while temperature at the area influenced by the rivers cooled at a rate of −0.15°C dec^{-1} over the period 1982–2014. The mere presence of a freshwater layer is able to modulate the warming observed at adjacent ocean locations since the coastal area is isolated from the rest of the Bay. This nearshore strip is the only part of the Bay where changes in SST depend on North Atlantic Oscillation (NAO) but not on North Atlantic SST represented by the Atlantic Multidecadal Oscillation (AMO). These different cooling-warming trends are even more patent over the last years (2002–2014) under atmospheric favorable conditions for plume enhancement. River runoff increased at a rate on the order of 120 $m^3s^{-1}dec^{-1}$ over that period and southwesterly winds, which favor the confinement of the plume, showed a positive and significant trend both in duration and intensity. Thus, the coastal strip has been observed to cool at a rate of −0.5°C dec^{-1}.

1. Introduction

It is an undeniable fact that ocean heat content and temperature have increased worldwide since mid-20th century [*Levitus et al*., 2000, 2005, 2012; *Belkin*, 2009]. Nevertheless, the rate of change is strongly dependent on the basin as described in *Levitus et al*. [2000]. Even inside the same basin, coastal areas have shown a different warming rate when compared with ocean areas located at the same latitude, which can be attributed to different phenomena. Some authors have found important differences between coast and ocean for areas under strong upwelling conditions [*Relvas et al*., 2009; *Santos et al*., 2011, 2012a, 2012b, 2012c; *deCastro et al*., 2009]. Other authors have attributed the observed differences to the presence and displacement of mesoscale structures like the Great Whirl [*Santos et al*., 2015]. Finally, other authors, [*Howden and Murtugudde*, 2001; *Vizy and Cook*, 2010; *Park et al*., 2011; *Materia et al*., 2012] linked the presence of rivers, as well as the presence of transitional water bodies such as coastal lagoons [e.g., *Kozlov et al*., 2014], to the different warming or cooling patterns found in some regions. For a full study on SST changes worldwide, the reader is referred to *Lima and Wethey* [2012], who detected that 71.6% of the world coastal locations have experienced a warming trend during the last three decades.

River plumes have a great impact on the characteristics of the adjacent seawater, also affecting the important economic activities associated to these areas. Plumes influence the morphodynamics and the ecological balance of the affected areas since they transport sediments, contaminants, organic material, and fresh water, among others. Therefore, changes in river plumes imply modifications in the physical, chemical, and biological characteristics of seawater. Physical modifications are associated with variations in circulation patterns, stratification, available light, or SST. Chemical modifications are linked to fluctuations in dissolved and particulate matter. These changes in the properties of seawater promote an associated biological impact modifying the distribution of the microorganisms as well as the abundance and composition of the species [*Alber*, 2002; *Cooley and Yager*, 2006; *Ffield*, 2007; *Azevedo et al*., 2008; *Belkin*, 2009; *de Boer et al*., 2009; *Vizy and Cook*, 2010; *Petus et al*., 2010, 2014]. Therefore, the analysis of the river plumes development results essential for these areas. Nevertheless, the track of the plumes is difficult because its displacement is

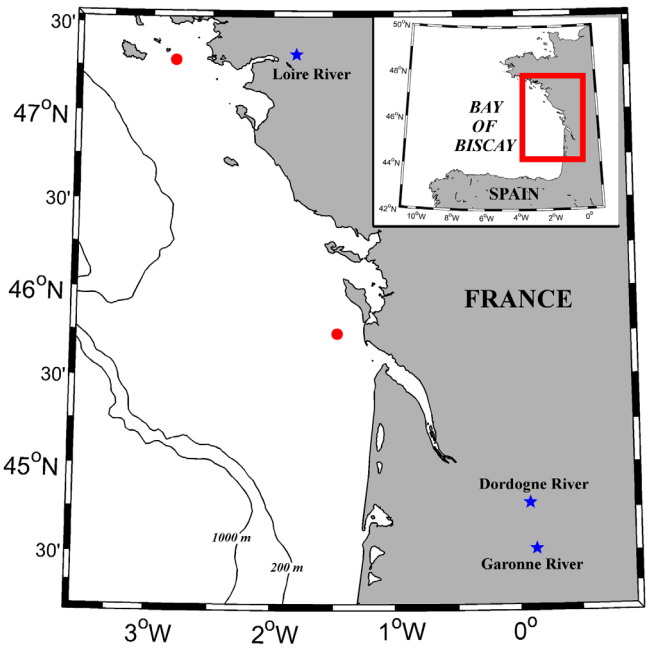

Figure 1. Bathymetry of the region under study. Contour lines represent, 200 and 1000 m isobaths. Red dots mark the location where wind was obtained. Blue asterisks mark the location where river discharge was sampled.

influenced by numerous parameters as outflow inertia, Coriolis effects, buoyancy, wind, tidal forcing, or topography [*Fong and Geyer*, 2001; *Lentz and Largier*, 2006; *Sousa et al.*, 2014]. Although each plume system has its own variability, some patterns are common. Generally, plumes formed by river discharge induce an anticyclonic gyre (in the Northern Hemisphere) with an associated coastal current. Plume development is associated with the momentum advection, the topography of the area [*Yankovsky and Chapman*, 1997; *Fong and Geyer*, 2002] as well as with Ekman transport when wind is considered [*Horner-Devine et al.*, 2015]. In general, upwelling favorable winds tend to displace the plume seaward as a consequence of offshore Ekman transport, whereas downwelling winds tend to compress the plume against the coast due to onshore Ekman transport [*Fennel and Mutzke*, 1997; *Whitney and Garvine*, 2005]. Tidal forcing can also influence the plume dynamics as a constraint factor in plume development [*Guo and Valle-Levinson*, 2007; *Vaz et al.*, 2009]. Plumes are usually larger and more turbid under low tides than under high tides [*Mendes et al.*, 2014]. Moreover, spring-neap tidal cycle also can generate changes in plume spreading in rivers preceded by large estuaries [*Uncles et al.*, 2002].

The Bay of Biscay is located in the Northeastern Atlantic Ocean covering the West coast of France and the Northern coast of Spain. The French continental shelf is characterized by a width that varies between 60 and 160 km widening northward (Figure 1). Numerous studies have focused on SST trends in the area since 1970s [*Koutsikopoulos et al.*, 1998; *Planque et al.*, 2003; *Llope et al.*, 2006; *Fontán et al.*, 2008; *Gómez-Gesteira et al.*, 2008; *deCastro et al.*, 2009; *Michel et al.*, 2009a,b; *Goikoetxea et al.*, 2009; *García-Soto and Pingree*, 2012; *Costoya et al.*, 2015]. All these studies have shown a clear warming trend, whose intensity is dependent on temporal and spatial scales. In this way, warming intensity is different depending on the season [e.g., *deCastro et al.*, 2009] and on the area under scope [e.g., *Gómez-Gesteira et al.*, 2008; *Michel et al.*, 2009b; *Costoya et al.*, 2015]. In addition, the type of data (in situ, simulations or reanalysis data) employed to carry out the studies can also modify slightly the intensity of warming. Thus, for example, *Michel et al.* [2009a] detected a warming trend of 0.22°C dec^{-1} and 0.37°C dec^{-1} by means of ORCA simulations and reanalysis data, respectively.

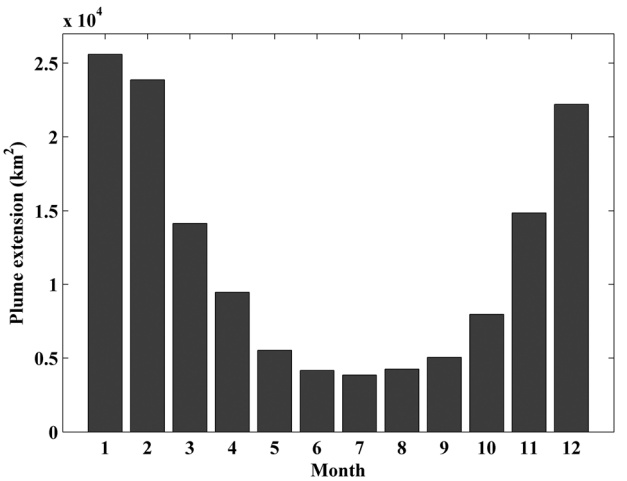

Figure 2. Monthly mean area (km^2) occupied by the turbid plume formed by Loire and Gironde Rivers discharges over the period 2002–2014.

The main freshwater inputs affecting this area are provided by the discharge of

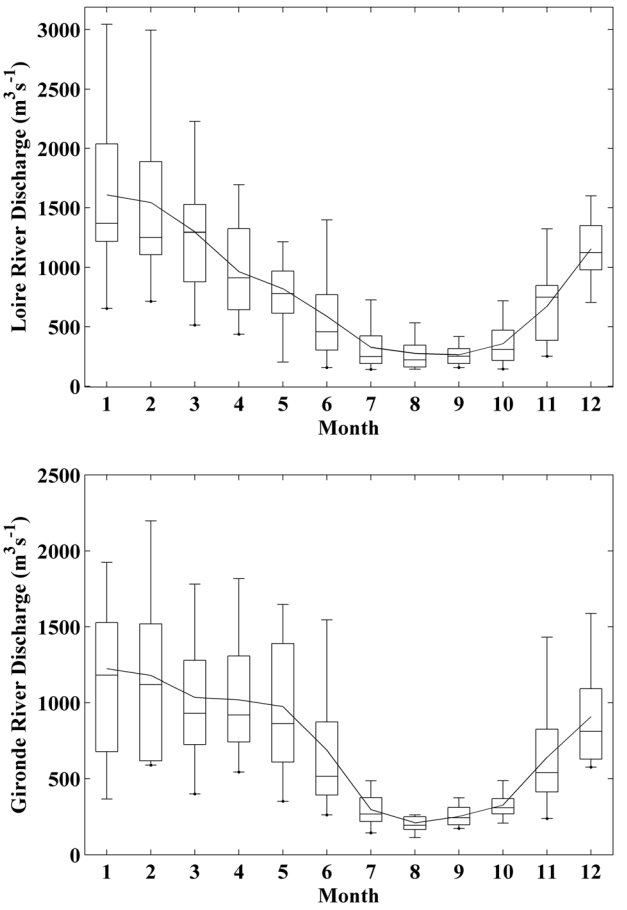

Figure 3. Annual hydrologic cycle variability (m^3s^{-1}) for (a) Loire and (b) Gironde runoff over the period 2002–2014. Solid black line represents the monthly average flow and the line inside each box represents the median for each month. Lower and upper whiskers show minimum and maximum river flow, respective, while lower and upper box indicate first and third quartiles, respectively.

Loire and Gironde Rivers [*Puillat et al.*, 2004]. Turbid plumes generated by both rivers can merge forming a great plume under high discharge conditions due to the synchronism of both rivers [*Koutsikopoulos and Le Cann*, 1996; *Lazure and Jegou*, 1998]. The Loire River has a length of about 1020 km from Mont Gerbier de Jonc, in the Massif Central, to Nantes at St Nazaire. Its basin occupies about 117,000 km^2 with a mean flow of ~900 m^3s^{-1}. Gironde River (estuary) is formed by the contributions of Garonne and Dordogne Rivers. Garonne River has a length of ~600 km from Aran Valley, in the Pyrenees (Spain), to the Gironde estuary, in Bec d'Ambès, north of Bordeaux. Its basin occupies about 61,000 km^2 with a mean flow of ~500 m^3s^{-1}. Dordogne River has a length of ~485 km from the Puy of Sancy, in the mountains of Auvergne, to the Gironde Estuary. Its basin occupies about 24,000 km^2 with a mean flow of ~250 m^3s^{-1}.

Previous studies about turbid plumes in the Bay of Biscay have been conducted by means of numerical models [*Lazure and Jegou*, 1998], in situ data [*Kelly-Gerreyn et al.*, 2006; *Gónzalez-Nuevo and Nogueira*, 2014], satellite imagery [*Petus et al.*, 2010, 2014], or by combining several of these methods [*Ferrer et al.*, 2009]. These studies have highlighted that, although Loire and Gironde plumes are usually oriented to the NW due to Coriolis effect, the development of both plumes depends mainly on the variability of river runoff and winds [*Lazure and Jegou*, 1998]. Winds over the French continental shelf are characterized by a marked interannual variability. Thus, southwesterly winds prevail from October to March and northwesterly winds from April to September [*Puillat et al.*, 2004, 2006]. In addition, surface circulation is also important since it affects the plume displacement. Currents over the shelf are conditioned by wind, density gradients, and tides [*Pingree and Le Cann*, 1989]. Overall, a poleward circulation prevails during winter in this area [*Charria et al.*, 2013], contributing to the NW orientation of plumes.

The Moderate Resolution Imaging Spectroradiometer (MODIS) onboard Aqua and Terra satellites provides a unique and valuable data set to analyze river plumes. On the one hand, radiance measurements provide information about the extent and features of the plume. On the other hand, SST measurements allow identifying microscale warming trends that can be correlated with the plume. Ocean color satellite imagery has been used to analyze river plume development. It allows discerning between turbid water related to river discharge and ocean water due to their different optical properties [*Dzwonkowski and Yan*, 2005; *Shi and Wang*, 2009; *Valente and da Silva*, 2009; *Saldías et al.*, 2012]. Thus, several studies related to turbid plumes have been conducted using this technology all over the world [*Walker et al.*, 2005; *Palacios et al.*, 2009; *Molleri et al.*, 2010; *Petus et al.*, 2010; *Mendes et al.*, 2014; *Fernández-Nóvoa et al.*, 2015]. In addition, satellite technology has also been used to analyze sea surface temperature (SST) in areas influenced by river plumes because of the high spatial and temporal resolution provided [*Walker et al.*, 2005; *de Boer et al.*, 2009; *Hopkings et al.*, 2013].

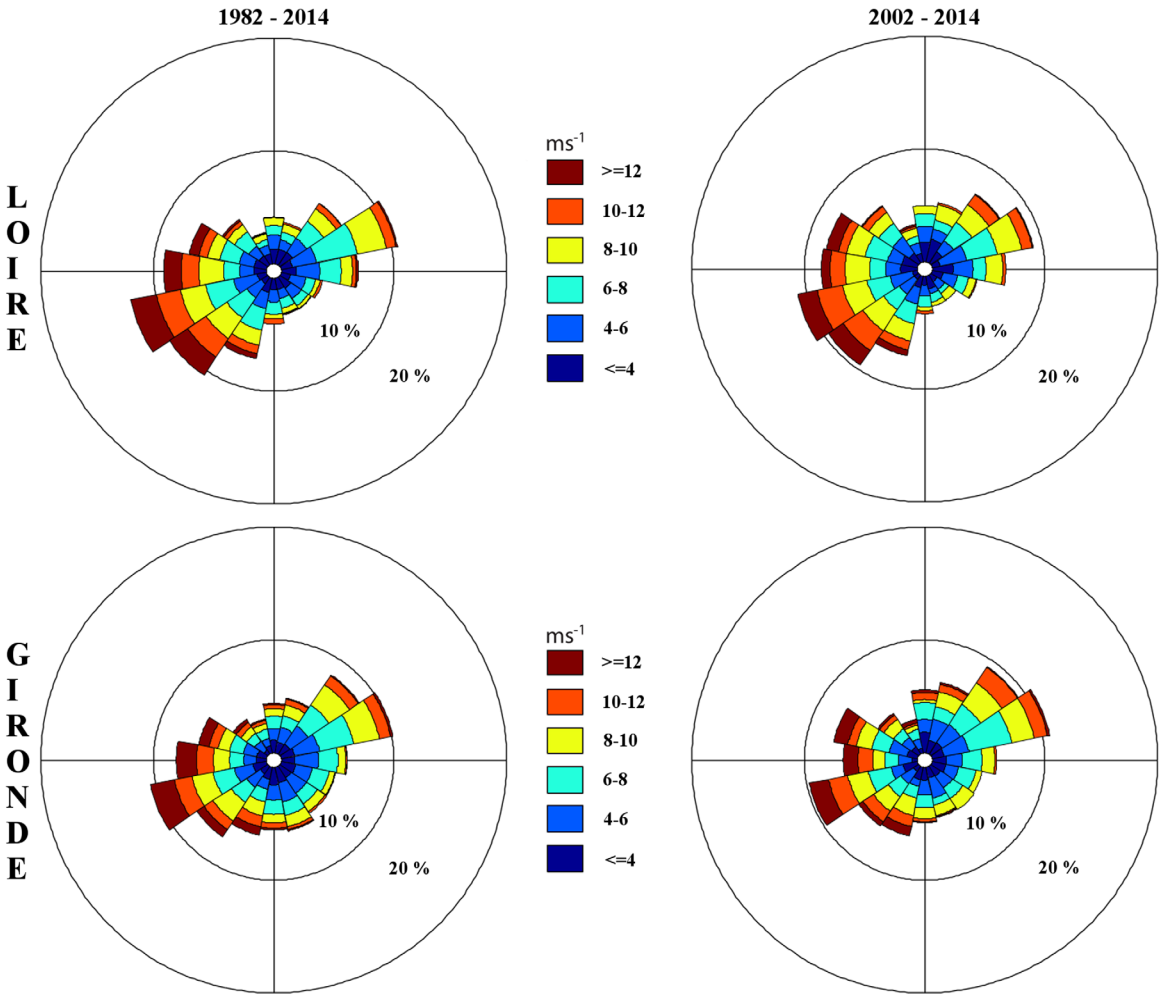

Figure 4. Wind rose (ms^{-1}) representing DJF winds near (top plots) Loire and (bottom plots) Gironde mouths over the periods (left) 1982–2004 and (right) 2002–2014.

The aim of this study is to analyze the influence of the Loire and Gironde river plume on SST trends on the Atlantic part of the French continental shelf (eastern Bay of Biscay, 0.6°–36.6°W, 44.2–47.8°W) during months of maximum plume extension. The analysis will be carried out in terms of radiance and SST measurements (MODIS), combined with SST data provided by the Advanced Very High Resolution radiometer ($OISST_{1/4}$) and reanalysis data (wind, heat fluxes, . . .) provided by the Climate Forecast System Reanalysis (CFSR). The study combines the high resolution and short duration provided by MODIS with the moderate resolution and long duration of $OISST_{1/4}$. SST trends will be correlated with the main drivers (river discharge, wind variability, and teleconnection patterns) that affect the river plume.

2. Databases and Methodology

2.1. MODIS: Daily Turbidity and SST Data (2002–2014)

As we mentioned above, MODIS is a sensor located onboard Aqua and Terra satellites which provides information of several parameters. Normalized water-leaving radiance (nLw) and Sea Surface Temperature (SST) using 11–12 μm channels were selected to develop this study. Both data sets with a resolution of 1 km were retrieved from the NASA Ocean Color web site (http://oceancolor.gsfc.nasa.gov). Daytime (nLw) data were considered to evaluate the plume development pattern because water leaving radiance data are only measured during the day. Nighttime SST data, acquired by infrared bands, were considered because they have fewer fluctuations due to their independence of the solar radiation.

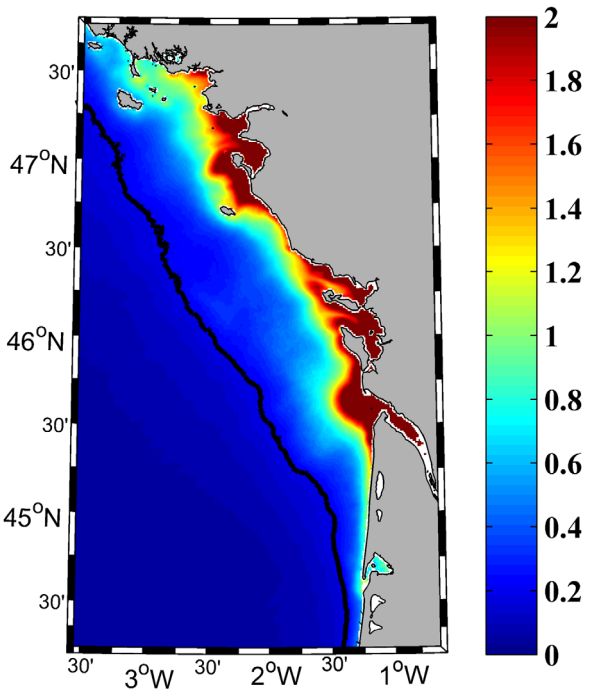

Figure 5. Mean DJF turbid plume (mWcm^{-2}μm^{-1}sr^{-1}) calculated over the period 2002–2014. The contour line corresponds to the turbid threshold (0.2 mWcm^{-2}μm^{-1}sr^{-1}).

MODIS allows selecting several values of normalized water-leaving radiance (nLw). Some nLw bands (412, 443, 469) were discarded because their high depth of penetration. The characterization of the river plume formed by Loire and Gironde Rivers was carried out by means of several nLw values (555, 645) obtaining a similar behavior. Although the 555 nm band (nLw555) provides one of the strongest turbid signals to determine river plumes [*Nezlin and DiGiacomo*, 2005; *Nezlin et al*., 2005; *Saldías et al*., 2012], the 645 nm band was selected because it has a lower penetration that allows analyzing shallow areas preventing bottom influence. A turbid threshold of 0.2 mWcm^{-2}μm^{-1}sr^{-1} was obtained to delimit the turbid river plume for this band following the methodology described in *Fernández-Nóvoa et al*. [2015]. SST data were obtained using 11–12 μm channels since these bands are located close to the maximum of the Earth's emission and have larger bandwidth than other available channels [*Reinart and Reinhold*, 2008]. This SST product has been shown to be suitable to analyze water surface temperatures in previous studies [*Barré et al*., 2006; *Reinart and Reinhold*, 2008; *Chavula et al*., 2009]. MODIS SST data present a closely relation to in situ data in coastal zones, representing a good choice to estimate the sea surface temperature of these areas [*Chavula et al*., 2009]. Temperature measurement takes place in the superficial part of the sea, therefore the possible bottom influence is not a problem even in very shallow areas [*Barré et al*., 2006]. In addition, to avoid possible problems in the water-land interface, a mask was applied to the pixels located in that area for both products (nLw and SST).

Daily nLw645 and SST images from MODIS-Aqua and MODIS-Terra were merged following *Mendes et al*. [2014]. This allows obtaining a larger number of available pixels increasing the consistency of the study. These merged images were then interpolated into a regular mesh (0.01° × 0.01°). Monthly SST trends were calculated assuming linear regression.

2.2. OISST$_{1/4}$ Data (1982–2014)

Daily SST values and their associated errors were also obtained from the OISST$_{1/4}$ daily SST database [*Reynolds et al*., 2007]. Only data from the AVHRR sensor was used since it is located on board NOAA polar-orbiting satellites and provides an uninterrupted SST data series since March 1981 from the same class of instrument [*Casey et al*., 2010]. In addition, this database uses in situ data from ships and buoys to construct a regular global grid by means of a special form of kriging called Optimal Interpolation. This procedure retains large-scale correlation structures and allows assimilating very sparse data coverage [*Reynolds*, 2009; *Reynolds and Chelton*, 2010]. Version 2 of this SST product was selected in this study. It includes bias adjustments of satellite and ship data using buoys data. Daily files with a spatial resolution of 0.25° × 0.25° were retrieved from the NOAA website (http://www.ndc.noaa.gov/sst/). Daily SST values were averaged at monthly scale in order to calculate SST trends assuming linear regression.

Two SST products (MODIS and OISST$_{1/4}$) were used to carry out this study. Both products are mainly constructed by means of SST data collected by infrared sensors (MODIS and AVHRR sensors). In fact, MODIS sensor, which provides a higher spatial resolution and also a greater spectral resolution, is considered a successor of AVHRR sensor. The main difference is that MODIS database only uses remote sensing data, while OISST$_{1/4}$ database also includes data from ships and buoys that are used to prevent biases in satellite data with a post processing procedure to construct a global regular grid. Thus, the study combines the

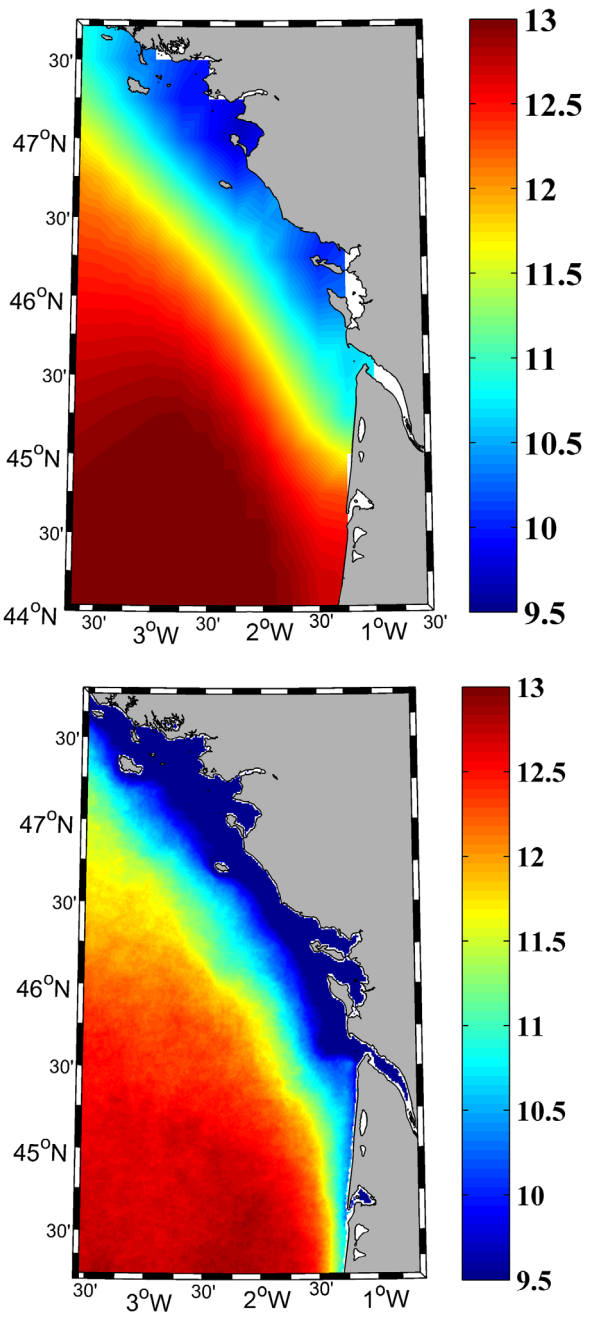

Figure 6. Mean DJF SST (°C) calculated over the period 2002–2014; (a) $OISST_{1/4}$ (b) MODIS.

high-resolution and short-duration provided by MODIS with the moderate resolution and long duration of $OISST_{1/4}$.

2.3. CFSR: Wind and Heat Fluxes Data (1982–2014)

Wind and heat fluxes data were obtained from NOAA's National Operational Model Archive and Distribution System (NOMADS), which is maintained at NOAA's National Climatic Data Center (NCDC) [*Saha et al*., 2010]. The used database was the Climate Forecast System Reanalysis (CFSR) developed by NOAA's National Centers for Environmental Prediction (NCEP) (http://rda.ucar.edu/pub/cfsr.html). CFSR provides a 0.3° × 0.3° × 6 h resolution, covering the atmosphere, ocean, sea ice and land.

CFSR wind data were chosen because it presents a great correlation with buoy measurements [*Álvarez et al*., 2014]. Wind data at a reference height of 10 m were daily averaged for two locations near Gironde and Loire mouths (Figure 1, red dots).

Heat fluxes (shortwave, longwave, latent heat, and sensible heat) were also obtained from the CFSR database at monthly scale. The net heat flux (Q_T) through the ocean surface was calculated following equation (1):

$$Q_T = Q_{SW} + Q_{LW} + Q_S + Q_L \quad (1)$$

where Q_{SW} is the shortwave flux, Q_{LW} is the longwave flux, Q_S is the sensible heat flux, and Q_L is the latent heat flux. A negative (positive) heat flux implies that ocean is losing (gaining) heat.

2.4. River Discharge Data

Daily runoff data for Loire and Gironde Rivers were obtained from the Banque Hydro French Database (http://www.hydro.eaufrance.fr/). River runoff is available over the period 1997–2014 for the Gironde and 1982–2014 for the Loire. The Gironde discharge was obtained as the sum of Dordogne and Garonne Rivers discharge. Daily data were averaged at monthly scale. River discharge data were sampled at the positions marked with blue asterisks in Figure 1.

2.5. NAO and AMO Indices (1982–2014)

The Atlantic Multidecadal Oscillation (AMO) and the teleconnection index for the North Atlantic Oscillation (NAO) were obtained from the Climate Prediction Center at the National Center of Environmental Prediction (http://www.cpc.noaa.gov). NAO is the most prominent teleconnection pattern in the Eastern North Atlantic region during winter [*Barnston and Livezey*, 1987]. It consists of a dipole with one center located over Greenland and the other over a region spanning between 35 and 40°N, in the central North Atlantic. The difference in geopotencial anomalies between both regions is used to calculate NAO index. AMO is a mode of

multidecadal variability in SST occurring in the North Atlantic Ocean. It is calculated from averaging SST anomalies in the Atlantic north of the equator [*Enfield et al.*, 2001].

3. Results

The monthly area occupied by the turbid plume generated by Loire and Gironde Rivers (averaged from 2002 to 2014) is shown in Figure 2. River plume extension is higher from December to February with values over 25,000 km^2. In general, those months are characterized by high river discharges (surpassing 1000 m^{3}s^{-1} for both rivers) as shown in Figure 3. However, there are other months (especially spring months) characterized by high river discharges where the river plume is considerably smaller. This fact implies that other factors besides the river discharge can also modulate the river plume. The second main factor that conditions the extension of the river plume is wind [*Mendes et al.*, 2014; *Fernández-Nóvoa et al.*, 2015]. Wind direction is mainly southwesterly from December to February as shown in Figure 4. Taking into account the coast orientation, southwesterly winds tends to accumulate material provided by river discharge near coast and to decrease cross-shore transport and dilution [*Chao*, 1988; *Mendes et al.*, 2014]. This behavior favors the retention and maintenance of the plume on a large area. Due to this fact, the further analysis will be focus on December–February (DJF) when the extent of the plume attains the highest values.

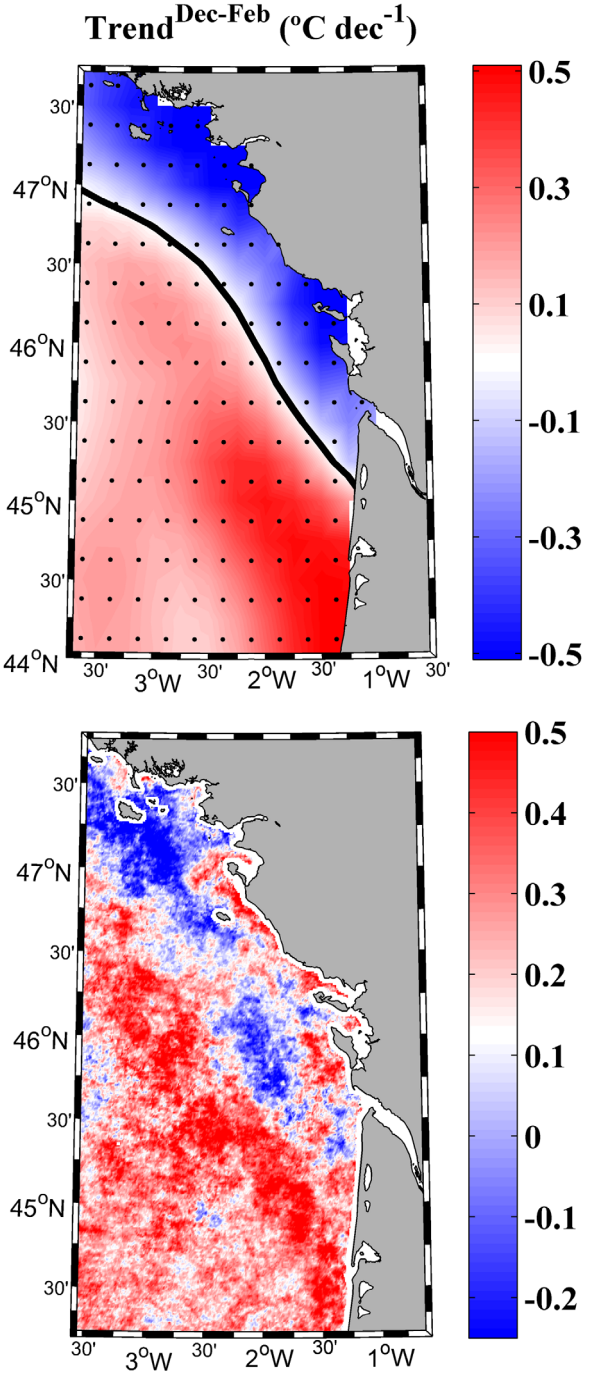

Figure 7. DJF SST trends (°C dec^{-1}) calculated over the period 2002–2014; (a) OISST$_{1/4}$. (b) MODIS. Contour line corresponds to null trend. Black dots represent grid points with significance higher than 90%.

The mean DJF plume averaged over the period 2002–2014 is shown in Figure 5. It has an offshore extension of 100 km and maximum turbid values on the order of 2 mWcm^{-2} μm^{-1} sr^{-1} near Loire and Gironde estuaries. In addition, a band of high turbid values (exceeding 1 mWcm^{-2}μm^{-1}sr^{-1}) can be observed near coast between Loire and Gironde Rivers. Dark solid line corresponds to the threshold of 0.2 mWcm^{-2} μm^{-1} sr^{-1} mentioned above.

The mean DJF SST field calculated from OISSST$_{1/4}$ data and averaged over the period 2002–2014 is shown in Figure 6a. Minimum values (close to 9.5°C) are located near the mouth of both rivers. In addition, a band with low temperatures (below 10.5°C) can also be observed near coast between Loire and Gironde estuaries. This fringe of low temperature is very similar to the fringe of high turbid values in the area occupied by

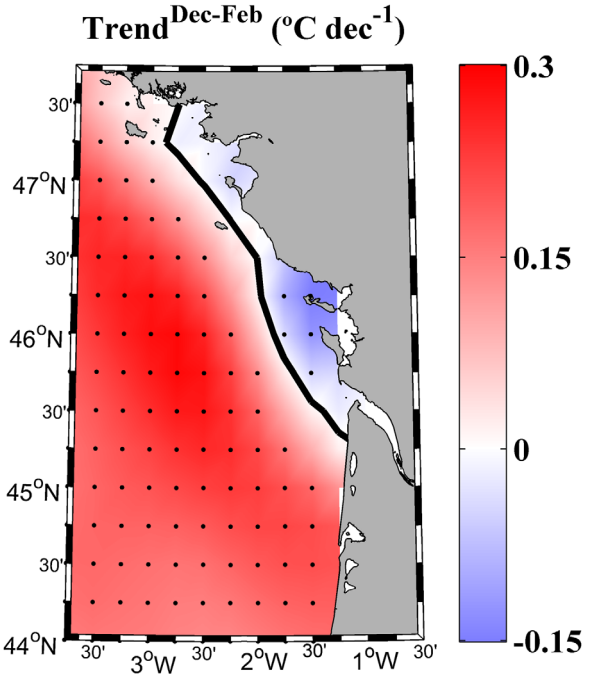

Figure 8. DJF SST trends (°C dec^{-1}) calculated over the period 1982–2014 with OISST$_{1/4}$ data. Contour line corresponds to null trend. Black dots represent grid points with significance higher than 90%.

the plume (Figure 5), which suggest that the coldest SST values are related to the distribution of the turbid plume. In fact, there is a considerable difference (greater than 3°C) between the area more influenced by the turbid plume, with values below 10°C, and the area outside the plume influence, with values above 13°C. The mean DJF SST field calculated from MODIS data over the same period (Figure 6b) is very similar to the one calculated from OISSST$_{1/4}$ data although with small differences in some areas. Thus, for example, a band of low temperatures close to 9.5°C was detected along the whole coast and not only at Loire and Gironde estuaries as provided by OISST$_{1/4}$.

DJF SST trends were calculated over the period 2002–2014 using OISSST$_{1/4}$ (Figure 7a) and MODIS (Figure 7b) data. DJF SST trends calculated using the OISST$_{1/4}$ show a continuous cooling along the French coast north of 45°N. The highest cooling (∼−0.5°C dec^{-1}) was observed close to Loire estuary and north of Gironde estuary. This cooling strip contrasts with the warming observed for the rest of the area. In spite of the limited length of the series (only the period with available MODIS data were considered), trends are observed to be significant at 90%. DJF SST trends calculated from MODIS data (Figure 7b) show a similar pattern with a moderate cooling in most of the area influenced by the plume and a warming, reaching values close 0.5°C dec^{-1}, outside the river plume area. Obviously, the signal is noisier than the one calculated with OISST$_{1/4}$. We should note that MODIS data are obtained at a much finer resolution (∼0.01° instead of 0.25°) and have not been interpolated in such a way that voids due to cloud coverage or satellite malfunction can limit the number of available data at some grid point and bias trends at those locations. Despite these constraints that limit the efficiency of MODIS data to calculate SST trends, an almost continuous strip of cooling was observed between Loire and Gironde estuaries. The comparison of SST trends from OISST$_{1/4}$ and MODIS data show that cooling is observed in the area under plume influence independently of the database.

Both databases have shown similar mean and trend patterns (Figures 6 and 7). This allows extending back the period of study to the total length of OISST$_{1/4}$ database (1982–2014). The pattern depicted in Figure 8 is similar to the one described in Figure 7 but covering a longer period. Overall, warming (∼0.3°C dec^{-1}) was observed in most of the area under scope, with the exception of small nearshore zones close to the mouths of Gironde and Loire, where a maximum cooling rate of approximately −0.15°C dec^{-1} was observed. In summary, coastal cooling is maintained even when the period under study is extended to the last 30 years. This phenomenon is not a particular event that occurs only during the short period of time covered by MODIS data.

DJF trends in total heat flux (Figure 9a) calculated over the period 1982–2014 show a similar pattern to the one observed for DJF SST trends (Figure 8). Ocean trends range from −7 to −11 W m^{-2} dec^{-1} whilst the trend in the nearshore strip ranges from −3 to −5 W m^{-2} dec^{-1}. Note that ocean loses heat during DJF, so a negative trend means that the loss rate has increased. So, ocean is losing heat now at a higher rate than three decades ago. Following *Somavilla et al.* [2009], the radiative term can be neglected in DJF because shortwave and longwave fluxes balance each other. In this sense, changes in the total heat flux are mainly due to changes in the turbulent term (latent and sensible fluxes). In addition, *Somavilla et al.* [2009] also state that DJF sensible heat flux is close to zero being negligible when compared with the latent heat flux. Thus, the pattern depicted in Figure 9b, where only latent heat flux has been considered, is very similar to

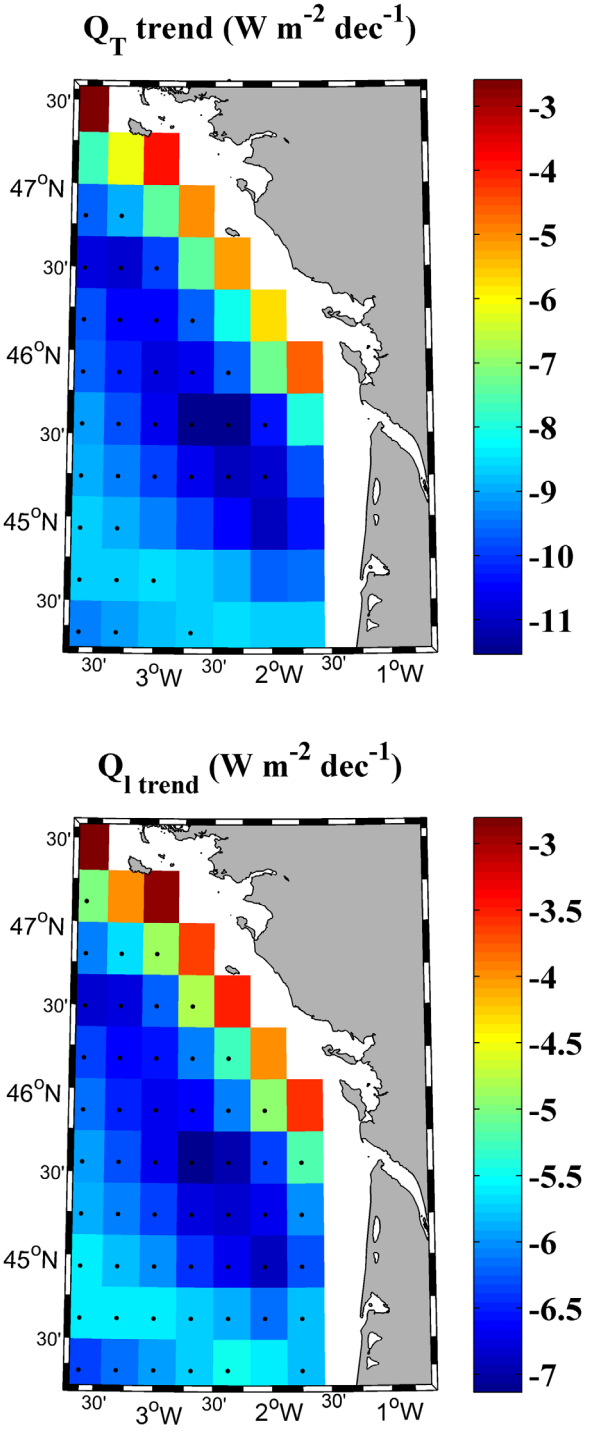

Figure 9. DJF trends in heat fluxes (W m^{-2} dec^{-1}) calculated over the period 1982–2014 with CFSR data. (a) Total heat; (b) Latent heat. Black dots represent grid points with significance higher than 95%.

the one depicted in Figure 9a for the total heat fluxes. In both cases (total heat and latent heat), only ocean trends are statistically significant at 95%.

Differences between ocean and coastal areas can be analyzed in terms of oceanic (AMO) and atmospheric (NAO) indices. The influence of AMO on SST anomaly was studied (Figure 10a) for DJF over the period 1982–2014. The correlation between both signals is close to zero in the area affected by the river plume while it is significantly positive for the rest of the region. This fact evidences that the nearshore strip influenced by Loire and Gironde discharges follows a different SST behavior when compared to the oceanic part of the bay. We should note that AMO represents the SST anomaly of the North Atlantic. The lack of correlation with the coastal zone close to Loire and Gironde Rivers proves that the SST at that particular area is more dependent on coastal than on oceanic features. The influence of NAO index on SST anomaly over the area under scope was also considered under the temporary conditions described above. Figure 10b shows significant positive correlation ($>$0.4) between SST NAO index for the months under study only in the area influenced by the river plume, which evidences its influence on coastal SST. The Bay of Biscay is a transition zone located between the centers that defined NAO index [*Massei et al.*, 2010]. This fact explains the lack of significant correlation for most of the bay. Winter NAO index influences the weather conditions of the North Atlantic in terms of heat, wind, and rainfall [*Hurrell et al.*, 2003; *Larroudé et al.*, 2013]. So, the relationship between NAO and SST in the area influenced by river plume is complex since there different mechanisms can be involved, such as wind direction that influences the extension of river plume or precipitation, which is related to river flow. Therefore, changes in the atmospheric circulation pattern in the North Atlantic can influence SST variability in the oceanic area affected by Loire and Gironde river plumes throughout variations in wind direction and changes in precipitation.

4. Discussion

The area affected by Gironde and Loire Rivers has shown different winter SST trends when compared with the adjacent oceanic part of the Bay of Biscay. Overall, SST tends to warm at the oceanic part and to cool slightly at the part influenced by rivers (Figure 8). This fact is corroborated by heat flux patterns and by the

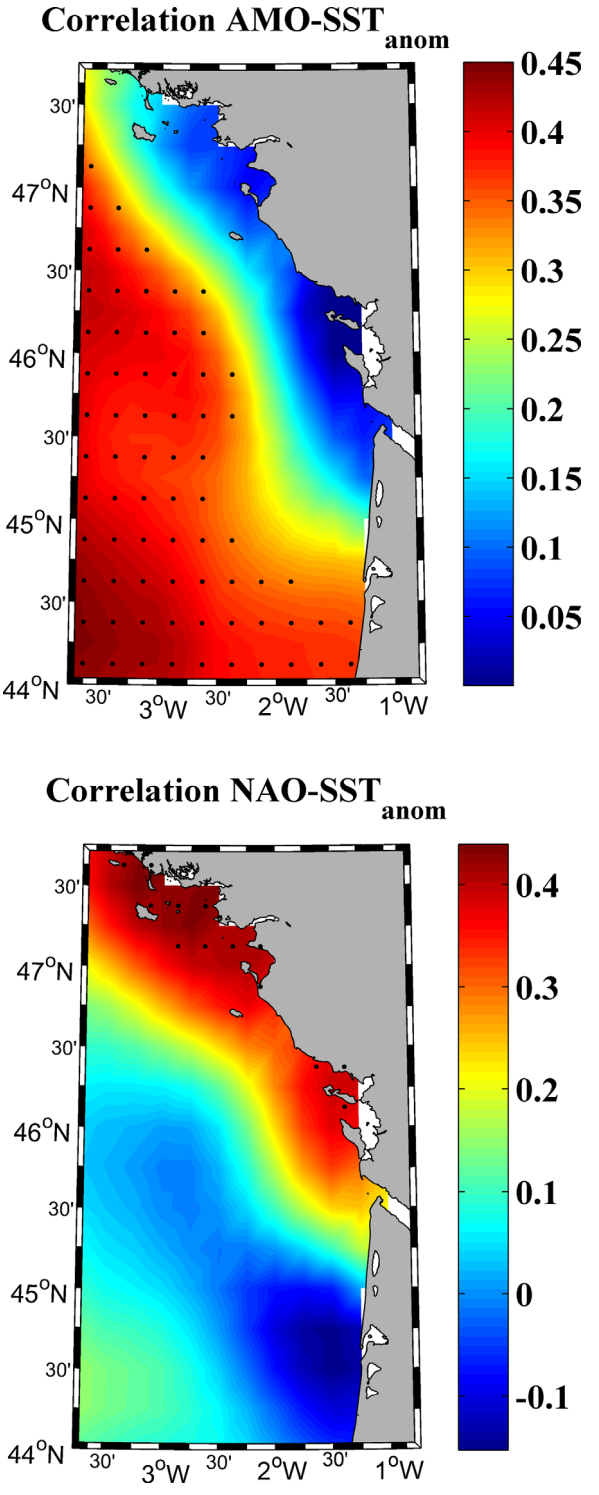

Figure 10. Correlation between DJF NAO (a), DJF AMO (b) indices and DJF SST anomaly over the period 1982–2014. Black dots represent grid points with significance higher than 95%.

dependence on atmospheric and oceanic indices. Thus, the coastal area where both rivers flow into the ocean is the only part of the Bay where SST depends on NAO but not on the SST of the North Atlantic represented by AMO. In the same way, Figures 7 and 8 show that coastal cooling is limited to the north of 45°. Previous studies that analyzed wintertime SST trends in this coastal area over a similar period are not conclusive. *Gómez-Gesteira et al.* [2008] mentioned that coastal warming is negligible along the French coast over the period 1985–2005 during winter and fall, while they observed a high increase during spring and summer. However, *Planque et al.* [2003] showed that warming was greater in the southeastern corner of the Bay during winter.

In a wider context, there are several drivers that can cause different coastal SST trends when compared with the ones observed at adjacent oceanic areas. Possibly, coastal upwelling is the most studied cause [*Relvas et al.*, 2009; *Santos et al.*, 2011, 2012a, 2012b, 2012c; *deCastro et al.*, 2009]. Nevertheless, upwelling is not a key phenomenon in the area, especially in winter. The southeastern corner of the Bay is characterized by a high continental influence during summer due to the concavity of this area [*Valencia et al.*, 2003, 2004; *Costoya et al.*, 2015]. However, advection from land to ocean was also discarded in the area following *Cattiaux et al.* [2011]. Different authors have identified the presence of large rivers as the main cause of unusual cooling [*Howden and Murtugudde*, 2001] or warming [*Belkin*, 2009; *Vizy and Cook*, 2010; *Park et al.*, 2011; *Materia et al.*, 2012]. The importance of the river discharge can be put into context for the particular case under study since the combined discharge of both rivers ($\sim$2500 m^3s^{-1}) is higher than the flow per kilometer of coast of upwelled water observed for the main upwelling systems over the world [*Patti et al.*, 2008].

The mechanism proposed by different authors [*Belkin*, 2009; *Vizy and Cook*, 2010; *Park et al.*, 2011; *Materia et al.*, 2012] to explain the especially intense surface warming observed at certain areas affected by large rivers is based on the development of a buoyant surface layer that traps solar radiation and enhances vertical stratification. The mechanism is strengthened by positive feedback since the partially isolated surface layer is warmed by solar radiation that increases surface temperature which results in density decrease and hence

Table 1. Trends in Wind Intensity and Duration and in River Discharge[a]

		Area	2002–2014	1982–2014
SW winds	Duration (d dec^{-1})	Loire	11	–
		Gironde	13*	–
	Intensity (ms^{-1}dec^{-1})	Loire	1.6**	–
		Gironde	1.6**	–
River	Runoff (m^{3}s^{-1}dec^{-1})	Loire	126	−40
		Gironde	122	n/a

[a]Values with null trends are marked with –. Statistical significance at 95% || 99% is marked with * || **.

reinforcement of stratification. These previous studies are focused on spring-summer periods when riverine water is warmer than offshore water. A similar mechanism can be invoked in the present study. The river plume is much fresher and colder (Figure 6) than the surrounding water. In spite of the possible existence of a thermal inversion near surface [*Koutsikopoulos and Le Cann*, 1996], the stability of the water column is kept due to the continuous supply of freshwater. Overall, the surface water near coast is cooled by the atmosphere but vertical mixing is inhibited by density differences produced by near surface fresh water. Thus, in a context of global warming, offshore water warms at a much higher rate than near shore water. Here, the positive feedback mechanism mentioned for other areas is no longer valid since surface water tends to cool and surface density to increase. In addition, the combined discharge of both river is rather moderate when compared to the rivers considered in the studies mentioned above (Congo, Amazonas or Yangtze). Thus, in spite of the shallowness of the area, the zone affected by the river plume is much smaller than observed for those large rivers.

Previous research carried out at other locations [*Mendes et al*., 2014; *Fernández-Nóvoa et al*., 2015] has proved that the extension of the plume is strongly dependent on river runoff and prevailing winds. The role of winds in the area is also corroborated by different works [*Lazure and Jegou*, 1998; *Puillat et al*., 2004, 2006]. In the present case, changes in DJF river runoff over the period 1982–2014 can be considered negligible for Loire River (on the order of -40 m^{3}s^{-1}dec^{-1}). Actually, the observed trends are not statistically significant and strongly dependent on the length of the series. To remove or add a single year can drive the trend from positive to negative (or vice-versa). River runoff increases at a rate on the order of 120 m^{3}s^{-1}dec^{-1} (still not significant) when considering the last period (2002–2014), which coincides with a stronger coastal cooling as shown in Figure 7. As we mentioned above, the area affected by the plume has little horizontal mixing with the rest of the area due to the prevailing winds that tend to compress the plume decreasing the cross-shore transport and dilution [*Chao*, 1988; *Mendes et al*., 2014]. This behavior favors the retention and maintenance of the plume on a large area, partially isolated from the rest of the bay. Changes in the duration and intensity of prevailing DJF Southwesterly winds were also analyzed at the stations located close to the mouth of Gironde and Loire Rivers (Table 1). Null trends were observed for duration and intensity of these winds over the period 1982–2014. Nevertheless, trends are positive and significant (Table 1) when considering the short period 2002–2014. SW winds tend to intensify and be more frequent during this period. This results in a higher compression and retention of the plume near coast which, in turns, results in a more marked cooling in that area as depicted in Figure 7. Although tidal forcing also affects plume development, its influence on plume spreading is balanced over time because it has a cyclic effect on plume dynamics.

In summary, we can conclude that the extension of the plume has experienced little changes over the period 1982–2014. Thus, at coastal areas, the mere presence of a freshwater layer is able to modulate the warming observed at the adjacent ocean locations even in absence of significant changes in the properties of the plume like its extent or freshwater content. The ocean area warms while the coastal area suffers a light cooling with low significance. The mechanism is reinforced during periods when river discharge and SW winds are over their mean values (e.g., 2002–2014). This results in a significant cooling in the area influenced by freshwater input.

Acknowledgments
The authors thank the Ocean Biology Processing Group (Code 614.2) at the GSFC, 522 Greenbelt, MD 20771, for the production and distribution of the ocean color and SST data (http://oceancolor.gsfc.nasa.gov), the NOAA's National Centers for Environmental Prediction (NCEP) for the development of the database Climate Forecast System Reanalysis (CFSR) (http://rda.ucar.edu/pub/cfsr.html) and the database Optimum Interpolation Sea Surface Temperature (OISST) (https://www.ncdc.noaa.gov/oisst). This work was partially supported by Xunta de Galicia under the project "Programa de Consolidación e Estructuración de Unidades de Investigación Competitivas: Grupos de Referencia Competitiva (GRC2013-001) co-funded by the European Regional Development Fund (FEDER) and the Project EM2013/003. X. Costoya and D. Fernández-Nóvoa are supported by the Xunta de Galicia through the Plan Galego de investigación, innovación e crecemento 2011–2015 (Plan I2C) in collaboration with the International Campus do Mar (PRE/2012/431 and PRE/2013/395, respectively). F. Santos is supported by the Portuguese Science Foundation (FCT) through a Post-doctoral grant (SFRM/BDP/97320/2013).

References

Alber, M. (2002), A conceptual model of estuarine freshwater inflow management, *Estuaries*, *25*(6), 1246–1261.

Álvarez, I., M. Gómez-Gesteira, M. deCastro, and D. Carvalho (2014), Comparison of different wind products and buoy wind data with seasonality and interannual climate variability in the southern Bay of Biscay (2000–2009), *Deep Sea Res., Part II*, *106*, 38–48, doi:10.1016/j.dsr2.2013.09.028.

Azevedo, I. C., P. M. Duarte, and A. A. Bordalo (2008), Understanding spatial and temporal dynamics of key environmental characteristics in a mesotidal Atlantic estuary (Douro, NW Portugal), *Estuarine Coastal Shelf Sci.*, *76*, 620–633, doi:10.1016/j.ecss.2007.07.034.

Barnston, A. G., and R. E. Livezey (1987), Classification, seasonality and persistence of low-frequency atmospheric circulation patterns, *Mon. Weather Rev.*, *115*, 1083–1126, doi:10.1175/1520-0493(1987)115<1083:CSAPOL>2.0.CO;2.
Barré, N., C. Provost, and M. Saraceno (2006), Spatial and temporal scales of the Brazil-Malvinas Current confluence documented by simultaneous MODIS Aqua 1.1-km resolution SST and color images, *Adv. Space Res.*, *37*, 770–786, doi:10.1016/j.asr.2005.09.026.
Belkin, I. M. (2009), Rapid warming of large marine ecosystems, *Prog. Oceanogr.*, *81*, 207–213, doi:10.1016/j.pocean.2009.04.011.
Casey, K. S., T. B. Brandon, P. Cornillon, and R. Evans (2010), The past, present, and future of the AVHRR Pathfinder SST program, in *Oceanography From Space*, edited by J. F. R. Gower, V. Barale and L. Alberotanza, pp. 273–287, Springer, Netherlands.
Cattiaux, J., R. Vautard, and P. Yiou (2011), North-Atlantic SST amplified recent wintertime European land temperature extremes and trends, *Clim. Dyn.*, *36*(11–12), 2113–2128, doi:10.1007/s00382-010-0869-0.
Chao, S. Y. (1988), Wind-driven motion of estuarine plumes, *J. Phys. Oceanogr.*, *18*, 1144–1166.
Charria, G., P. Lazure, B. Le Cann, A. Serpette, G. Reverdin, S. Louazel, F. Batifoulier, F. Dumas, A. Pichon, and Y. Morel (2013), Surface layer circulation derived from Lagrangian drifters in the Bay of Biscay, *J. Mar. Syst.*, *109–110*, S60–S76, doi:10.1016/j.jmarsys.2011.09.015.
Chavula, G., P. Brezonik, P. Thenkabail, T. Johnson, and M. Bauer, (2009), Estimating the surface temperature of Lake Malawi using AVHRR and MODIS satellite imagery, *Phys. Chem. Earth*, *34*, 749–754, doi:10.1016/j.pce.2009.08.001.
Cooley, S. R., and P. L. Yager (2006), Physical and biological contributions to the western tropical North Atlantic Ocean carbon sink formed by the Amazon River plume, *J. Geophys. Res.*, *111*, C08018, doi:10.1029/2005JC002954.
Costoya, X., M. deCastro, M. Gómez-Gesteira, and F. Santos (2015), Changes in sea Surface temperature seasonality in the Bay of Biscay over the last decades (1982–2014), *J. Mar. Syst.*, *150*, 91–101, doi:10.1016/j.jmarsys.2015.06.002.
de Boer, G. J., J. D. Pietrzak, and J. C. Winterwerp (2009), SST observations of upwelling induced by tidal straining in the Rhine ROFI, *Cont. Shelf Res.*, *29*, 263–277, doi:10.1016/j.csr.2007.06.011.
deCastro, M., M. Gómez-Gesteira, I. Álvarez, and J. L. G. Gesteira (2009), Present warming within the context of cooling-warming cycles observed since 1854 in the Bay of Biscay, *Cont. Shelf. Res.*, *29*, 1053–1059, doi:10.1016/j.csr.2008.11.016.
Dzwonkowski, B., and X. H. Yan (2005), Tracking of a Chesapeake Bay estuarine outflow plume with satellite-based ocean color data, *Cont. Shelf Res.*, *25*, 1942–1958, doi:10.1016/j.csr.2005.06.011.
Enfield, D. B., A. M. Mestas-Nuñez, and P. J. Trimble (2001), The Atlantic multidecadal oscillation and its relation to rainfall and river flows in the continental U.S, *Geophys. Res. Lett.*, *28*(10), 2077–2080.
Fennel, W., and A. Mutzke (1997), The initial evolution of a buoyant plume, *J. Mar. Syst.*, *12*, 53–68, doi:10.1016/S0924-7963(96)00088-7.
Fernández-Nóvoa, D., R. Mendes, M. deCastro, J. M. Dias, A. Sánchez-Arcilla, and M. Gómez-Gesteira (2015), Analysis of the influence of river discharge and wind on the Ebro turbid plume using MODIS-Aqua and MODIS-Terra data, *J. Mar. Syst.*, *142*, 40–46, doi:10.1016/j.jmarsys.2014.09.009.
Ferrer, L., A. Fontán, J. Mader, G. Chust, M. González, V. Valencia, A. Uriarte, and M. B. Colling (2009), Low-salinity plumes in the oceanic region of the Basque Country, *Cont. Shelf Res.*, *29*, 970–984, doi:10.1016/j.csr.2008.12.014.
Ffield, A. (2007), Amazon and Orinoco River Plumes and NBC Rings: Bystanders or Participants in Hurricane Events?, *J. Clim.*, *20*, 316–333, doi:10.1175/JCLI3985.1.
Fong, D. A., and W. R. Geyer (2001), Response of a river plume during an upwelling favorable wind event, *J. Geophys. Res.*, *106*(C1), 1067–1084.
Fong, D. A., and W. R. Geyer (2002), The alongshore transport of freshwater in a surface-trapped river plume, *J. Phys. Oceanogr.*, *32*(3), 957–972, doi:10.1175/1520-0485(2002)032<0957:TATOFI>2.0.CO;2.
Fontán, A., V. Valencia, Á. Borja, and N. Goikoetxea, N (2008), Oceano-meteorological conditions in the SE Bay of Biscay for the period 2001–2005. A comparison with the last two decades, *J. Mar. Syst.*, *72*, 167–177, doi:10.1016/j.jmarsys.2007.08.003.
García-Soto, C., and R. D. Pingree, (2012), Atlantic multidecadal oscillation (AMO) and sea surface temperature in the Bay of Biscay and adjacent regions, *J. Mar. Biol. Assoc. U. K.*, *92*(2), 213–234.
Goikoetxea, N., Á. Borja, A. Fontán, M. González, and V. Valencia (2009), Trends and anomalies of the sea surface temperature during the last 60 years within the southeastern Bay of Biscay, *Cont. Shelf Res.*, *29*, 1060–1069, doi:10.1016/j.csr.2008.11.014.
Gómez-Gesteira, M., M. deCastro, I. Alvarez, and J. L. G. Gesteira (2008), Coastal sea surface temperature warming trend along the continental part of the Atlantic Arc (1985–2005), *J. Geophys. Res.*, *113*, C04010, doi:10.1029/2007JC004315.
Gónzalez-Nuevo, G., and E. Nogueira (2014), Temporal and spatial variability of river plumes in the NW and N Iberian shelf (1987-2007), *Cont. Shelf Res.*, *91*, 95–108, doi:10.1016/j.csr.2014.09.005.
Guo, X., and A. Valle-Levinson (2007), Tidal effects on estuarine circulation and outflow plume in the Chesapeake Bay, *Cont. Shelf Res. 27*, 20–42, doi:10.1016/j.csr.2006.08.009.
Hopkings, J., M. Lucas, C. Dufau, M. Sutton, J. Stum, O. Lauret, and C. Channelliere (2013), Detection and variability of the Congo River plume from satellite derived sea surface temperature, salinity, ocean colour and sea level, *Remote Sens. Environ.*, *139*, 365–385, doi:10.1016/j.rse.2013.08.015.
Horner-Devine, A. R., R. D. Hetland, and D. G. MacDonald (2015). Mixing and transport in coastal river plumes, *Annu. Rev. Fluid Mech.*, *47*, 569–594.
Howden, S. D., and R. Murtugudde (2001), Effects of river inputs into the Bay of Bengal, *J. Geophys. Res.*, *106*(C9), 19,825–19,843.
Hurrell, J. W., Y. Kushnir, G. Ottersen, and M. Visbeck (2003), An overview of the North Atlantic oscillation, *Geophys. Monogr. AGU*, *134*, 1–36.
Kelly-Gerreyn, B. A., D. J. Hydes, A. M. Jégou, P. Lazure, L. J. Fernand, I. Puillat, and C. Garcia-Soto (2006), Low salinity intrusions in the western English Channel, *Cont. Shelf Res.*, *26*, 1241–1257, doi:10.1016/j.csr.2006.03.007.
Koutsikopoulos, C., and B. Le Cann (1996), Physical processes and hydrological structures related to the Bay of Biscay anchovy, *Sci. Mar.*, *60*, 9–19.
Koutsikopoulos, C., P. Beillois, C. Leroy, and F. Taillefer (1998), Temporal trends and spatial structures of the sea surface temperature in the Bay of Biscay, *Oceanol. Acta*, *21*(2), 335–344.
Kozlov, I., I. Dailidienė, A. Korosov, V. Klemas, and T. Mingėlaitė (2014), MODIS-based sea surface temperature of the Baltic Sea Curonian Lagoon, *J. Mar. Syst.*, *129*, 157–165.
Larroudé, S., N. Massei, P. Reyes-Marchant, C. Delattre, and J. F. Humbert (2013), Dramatic changes in a phytoplankton community in response to local and global pressures: A 24-year survey of the river Loire (France), *Global Change Biol.*, *19*(5), 1620–1631.
Lazure, P., and A. M., Jegou (1998), 3D modelling of seasonal evolution of Loire and Gironde plumes on Biscay Bay continental shelf, *Oceanol. Acta*, *21*, 164–177.
Lentz, S. J., and J. Largier (2006), The influence of wind forcing on the Chesapeake Bay buoyant coastal current, *J. Phys. Oceanogr.*, *36*, 1305–1316.

Levitus, S., J. I. Antonov, T. P. Boyer, and C. Stephens (2000), Warming of the World Ocean, *Science*, *287*, 2225–2229, doi:10.1126/science.287.5461.2225.

Levitus, S., J. Antonov, and T. Boyer (2005), Warming of the world ocean, 1955-2003, *Geophys. Res. Lett.*, *32*, L02604, doi:10.1029/2004GL021592.

Levitus, S., et al. (2012), World ocean heat content and thermosteric sea level change (0-2000 m), 1955-2010, *Geophys. Res. Lett.*, *39*, L01603, doi:10.1029/2012GL051106.

Lima, F. P., and D. S. Wethey (2012), Three decades of high-resolution coastal sea surface temperatures reveal more than warming, *Nat. Commun.*, *3*, article 704, doi:10.1038/ncomms1713.

Llope, M., R. Anadón, L. Viesca, M. Quevedo, R. González-Quiros, and N. C. Stenseth (2006), Hydrography of the Southern Bay of Biscay shelf-break region: Interacting the multiscale physical variability over the period 1993–2003, *J. Geophys. Res.*, *111*, C09021, doi:10.1029/2005JC002963.

Massei, N., B. Laignel, J. Deloffre, J. Mesquita, A. Motelay, R. Lafite and A. Durand (2010), Long-term hydrological changes of the Seine River flow (France) and their relation to the North Atlantic Oscillation over the period 1950–2008, *Int. J. Climatol.*, *30*(14), 2146–2154.

Materia, S., S. Gualdi, A. Navarra, and L. Terray (2012), The effect of Congo River freshwater discharge on Eastern Equatorial Atlantic climate variability, *Clim. Dyn.*, *39*, 2109–2015, doi:10.1007/s00382-012-1514-x.

Mendes, R., N. Vaz, D. Fernández-Nóvoa, J. C. B. da Silva, M. deCastro, M. Gómez-Gesteira, and J. M. Dias (2014), Observation of a turbid plume using MODIS imagery: The case of Douro estuary (Portugal), *Remote Sens. Environ.*, *154*, 127–138, doi:10.1016/j.rse.2014.08.003.

Michel, S., A. M. Treguier, and F. Vandermeirsch (2009a), Temperature variability in the Bay of Biscay during the past 40 years, from an in situ analysis and a 3D global simulation, *Cont. Shelf Res.*, *29*, 1070–1087.

Michel, S., F. Vandermeirsch, and P. Lorance (2009b), Evolution of upper layer temperature in the Bay of Biscay during the last 40 years, *Aquat. Living Resour.*, *22*, 447–461, doi:10.1051/alr/29009054.

Molleri, G. S. F., E. M. L. Novo, and M. Kampel (2010), Space-time variability of the Amazon River plume based on satellite ocean color, *Cont. Shelf Res.*, *30*, 342–352, doi:10.1016/j.csr.2009.11.015.

Nezlin, N. P., and P. M. DiGiacomo (2005), Satellite ocean color observations of stormwater runoff plumes along the San Pedro Shelf (southern California) during 1997-2003, *Cont. Shelf Res.*, *25*(4), 1692–1711, doi:10.1016/j.csr.2005.05.001.

Nezlin, N. P., P. M. DiGiacomo, E. D. Stein, and D. Ackerman (2005), Stormwater runoff plumes observed by SeaWiFS radiometer in the Southern California Bight, *Remote Sens. Environ.*, *98*, 494–510, doi:10.1016/j.rse.2005.08.008.

Palacios, S. L., T. D. Peterson, and R. M. Kudela (2009), Development of synthetic salinity from remote sensing for the Columbia River plume, *J. Geophys. Res.*, *114*, C00B05, doi:10.1029/2008JC004895.

Park, T., C. J. Jand, J. H. Jungclaus, H. Haak, W. Park, and I. S. Oh (2011), Effects of the Changjiang river discharge on sea surface warming in the Yellow and East China Seas in summer, *Cont. Shelf Res.*, *31*, 15–22, doi:10.1016/j.csr.2010.10.012.

Patti, B., et al. (2008), Factors responsible for the differences in satellite-based chlorophyll a concentration between the major global upwelling areas, *Estuarine Coastal Shelf Sci.*, *76*(4), 775–786, doi:10.1016/j.ecss.2007.08.005.

Petus, C., G. Chust, F. Gohin, F. Doxaran, J. M. Froidefond, and Y. Sagarminaga (2010), Estimating turbidity and total suspended matter in the Adour River plume (South Bay of Biscay) using MODIS 250-m imagery, *Cont. Shelf Res.*, *30*, 379–392, doi:10.1016/j.csr.2009.12.007.

Petus, C., V. Marieu, S. Novoa, G. Chust, N. Bruneau, and J. M. Froidefond (2014), Monitoring spatio-temporal variability of the Adour River turbid plume (Bay of Biscay, France) with MODIS 250-m imagery, *Cont. Shelf Res.*, *74*, 35–49, doi:10.1016/j.csr.2013.11.011.

Pingree, R.D., and B. Le Cann (1989), Celtic and Armorican slope and shelf residual currents, *Prog. Oceanogr.*, *23*, 303–338.

Planque, B., P. Beillois, A. M. Jégou, P. Lazure, P. Petitgas, and I. Puillat (2003), Large-scale hydroclimatic variability in the Bay of Biscay: The 1990s in the context of interdecadal changes, *ICES Mar. Sci. Symp.*, *219*, 61–70.

Puillat, I., P. Lazure, A. M. Jégou, L. Lampert, and P. I. Miller (2004), Hydrographical variability on the French continental shelf in the Bay of Biscay, during the 1990s, *Cont. Shelf Res.*, *24*, 1143–1163, doi:10.1016/j.csr.2004.02.008.

Puillat, I., P. Lazure, A. M. Jégou, L. Lampert, and P. Miller (2006), Mesoscale hydrological variability induced by northwesterly wind on the French continental shelf of the Bay of Biscay, *Sci. Mar.*, *70*(S1), 15–26.

Reinart, A., and M. Reinhold (2008), Mapping surface temperature in large lakes with MODIS data, *Remote Sens. Environ.*, *112*, 603–611, doi:10.1016/j.rse.2007.05.015.

Relvas, P., J. Luis, and A. M. P. Santos (2009), Importance of the mesoscale in the decadal changes observed in the northern Canary upwelling system, *Geophys. Res. Lett.*, *36*, L22601, doi:10.1029/2009GL040504.

Reynolds, R. W. (2009), What's New in Version 2, NOAA/NCDC Rep., 10 pp., Asheville. [Available at http//www.ncdc.noaa.gov/oa/climate/research/sst/papers/whats_new_v2.pdf.]

Reynolds, R. W., and D. W. Chelton (2010), Comparisons of daily sea surface temperature analysis for 2007–08, *J. Clim.*, *23*, 3545–3562, doi:10.1175/2010JCLI3294.1.

Reynolds, R. W., T. M. Smith, C. Liu, D. B. Chelton, K. S. Casey and M. G. Schlax (2007), Daily high-resolution-blended analyses for sea surface temperature, *J. Clim.*, *20*(22), 5473–5496.

Saha, S., et al. (2010), The NCEP climate forecast system reanalysis, *Bull. Am. Meteorol. Soc.*, *91*(8), 1015–1057, doi:10.1175/2010BAMS3001.1.

Saldías, G. S., M. Sobarzo, J. Largier, C. Moffat, and R. Letelier (2012), Seasonal variability of turbid river plumes off central Chile based on high-resolution MODIS imagery, *Remote Sens. Environ.*, *123*, 220–233, doi:10.1016/j.rse.2012.03.010.

Santos, F., M. Gómez-Gesteira, M. deCastro, and I. Alvarez (2011), Upwelling along the western coast of the Iberian Peninsula: Dependence of trends on fitting strategy, *Clim. Res.*, *48*, 213–218, doi:10.3354/cr00972.

Santos, F., M. Gomez-Gesteira, M. deCastro, and I. Alvarez (2012a), Variability of coastal and ocean water temperature in the upper 700 m along the Western Iberian Peninsula from 1975 to 2006, *PLoS One*, *7*(12), 1–7, doi:10.1371/journalpone.0050666.

Santos, F., M. Gómez-Gesteira, M. deCastro, and I. Alvarez (2012b), Differences in coastal and oceanic SST trends due to the strengthening of coastal upwelling along the Benguela current system, *Cont. Shelf Res.*, *34*, 79–86, doi:10.1016/j.csr.2011.12.004.

Santos, F., M. deCastro, M. Gómez-Gesteira, and I. Alvarez (2012c), Differences in coastal and oceanic SST warming rates along the Canary upwelling ecosystem from 1982 to 2010, *Cont. Shelf Res.*, *47*, 1–6, doi:10.1016/j.csr.2012.07.023.

Santos, F., M. Gómez-Gesteira, M. deCastro, and J. M. Dias (2015), A dipole-like SST trend in the Somalia region during the monsoon season, *J. Geophys. Res. Oceans*, *120*, 597–607, doi:10.1002/2014JC010319.

Shi, W., and M. Wang (2009), Satellite observations of flood-driven Mississippi River plume in the spring of 2008, *Geophys. Res. Lett.*, *36*, L07607, doi:10.1029/2009GL037210.

Somavilla, R., C. González-Pola, C. Rodriguez, S. A. Josey, R. F. Sánchez, and A. Lavín (2009), Large changes in the hydrographic structure of the Bay of Biscay after the extreme mixing of Winter 2005, *J. Geophys. Res.*, *114*, C01001, doi:10.1029/2008JC004974.

Sousa, M. C., N. Vaz, I. Alvarez, M. Gómez-Gesteira, and J. M. Dias (2014), Modeling the Minho River plume intrusion into the Rias Baixas (NW Iberian Peninsula), *Cont. Shelf Res.*, *85*, 30–41, doi:10.1016/j.csr.2014.06.004.

Uncles, R. J., J. A. Stephens, and R. E. Smith (2002), The dependence of estuarine turbidity on tidal intrusion length, tidal range and residence time, *Cont. Shelf Res.*, *22*, 1835–1856, doi:10.1016/S0278-4343(02)00041-9.

Valencia, V., Á. Borja, A. Fontán, F. F. Pérez, and A. F. Ríos (2003), Temperature and salinity fluctuations in the Basque Coast (SE Bay of Biscay) from 1986 to 2000 related to the climatic factors, *ICES Mar. Sci. Symp.*, *219*, 340–342.

Valencia, V., J. Franco, A. Borja, and A. Fontán (2004), Hydrography of the southeastern Bay of Biscay, in *Oceanography and Marine Environment of the Basque Country*, edited by A. Borja and M. Collins, Oceanography Series, 70, 159–194, Elsevier, Amsterdam.

Valente, A. S., and J. C. da Silva (2009), On the observability of the fortnightly cycle of the Tagus estuary turbid plume using MODIS ocean colour images, *J. Mar. Syst.*, *75*(1), 131–137, doi:10.1016/j.jmarsys.2008.08.008.

Vaz, N., L. Fernandes, P. C. Leitão, J. M. Dias, and R. Neves (2009), The Tagus estuarine plume induced by wind and river runoff: Winter 2007 case study, *J. Coastal Res.*, *SI56*, 1090–1094.

Vizy, E. K., and K. H. Cook (2010), Influence of the Amazon/Orinoco Plume on the summertime Atlantic climate, *J. Geophys. Res.*, *115*, D21112, doi:10.1029/2010JD014049.

Walker, N. D., W. J. Wiseman Jr., L. J. Rouse Jr., and A. Babin (2005), Effects of river discharge, wind stress, and slope eddies on circulation and the satellite-observed structure of the Mississippi River Plume, *J. Coastal Res.*, *21(6)*, 1228–1244, doi:10.2112/04-0347.1.

Whitney, M. M., and R. W. Garvine (2005), Wind influence on a coastal buoyant outflow, *J. Geophys. Res.*, *110*, C03014, doi:10.1029/2003JC002261.

Yankovsky, A. E., and D. C. Chapman (1997), A simple theory for the fate of buoyant coastal discharges, *J. Phys. Oceanogr.*, *27*(7), 1386–1401, doi:10.1175/1520-0485(1997)027<1386:ASTFTF>2.0.CO;2.